Influence of the degree of a complex network on heat conduction

Kezhao Xiong,[1,2] Chunhua Zeng,[3,2,4] Zonghua Liu,[1,*] and Baowen Li[2,†]

[1]*Department of Physics, East China Normal University, Shanghai, 200062, People's Republic of China*

[2]*Department of Mechanical Engineering, University of Colorado, Boulder, Colorado 80309 USA*

[3]*Institute of Physical and Engineering Science, Kunming University of Science and Technology, Kunming 650500, People's Republic of China*

[4]*Department of Physics, Nanjing University, Nanjing 210093, People's Republic of China*

(Received 1 May 2018; revised manuscript received 19 July 2018; published 14 August 2018)

Devices made of nanotubes and nanowires networks are of great interest for applications and have caught increasing attention in recent years. In this work, we study heat conduction in a network model with nodes being atoms and links being one-dimensional chains of atoms. It is found that heat conduction in the complex network is fundamentally different from that of regular lattices. It depends very sensitively on the average degrees of complex networks and the degrees of nodes that are attached to the two heat baths. For example, when the two heat source nodes have the same degree k_0, the heat flux reaches a maximum at an optimized value of k_0 and decreases with the increase of the average degree $\langle k \rangle$. In other words, the source nodes with optimal degree k_0 and the sparse network are more favorable to heat flux. Thermal rectification effect is found when the two heat source nodes have different degrees or the network model has multiple heat source nodes. Theoretical analysis is provided to explain the numerical results.

DOI: 10.1103/PhysRevE.98.022115

I. INTRODUCTION

Study of heat conduction in low-dimensional [one- (1D) and two-dimensional (2D)] microscale [1,2] and nanoscale [3,4] systems has attracted increasing attention in past decades. On the one hand, study gives us a rather comprehensive, albeit not a complete, picture of heat conduction in a microscopic scale. For example, it is now known that the Fourier's law of heat conduction, i.e., heat flux is proportional to a temperature gradient applied to the system multiplied by a constant, might not be always true in micro- and nanoscale systems. The constant, called thermal conductivity, which is an intrinsic property of materials, is independent of geometry and size for bulk materials. However, it is found to be system size dependent in many 1D momentum-conserved systems, including lattices, toy models, and quasi-1D nanostructures like nanowires and nanotubes up to a certain length [5–9]. In the strict 2D systems, as revealed by the Fermi-Pasta-Ulam (FPU) model [10], the thermal conductivity exhibits a logarithmic size dependence. Recent intensive first principles calculations for graphene [11] indicate that the logarithmic relation seems to hold up to a certain length of $\sim$1 mm, as demonstrated by experiments [12]. On the other hand, study in particular of nonlinear system has led to the invention of different thermal circuits, such as thermal diode and thermal transistor, that have opened a new area for controlling and managing heat flow with an electronic analog [13].

These fundamental studies mainly focus on the thermal properties of an individual lattice or nanostructure such as a 1D lattice or a single nanowire or nanotube. However, for practical applications, a single nanowire or nanotube is extremely difficult to assembly and to control and manipulate. Usually, people try to make devices from networks of nanowires and nanotubes [14], which find applications in many fields, such as large-scale transparent conductors, transistors, sensors, and even flexible electronics [15,16].

Therefore, the study of physical properties such as electronic conduction and thermal conduction of the networks of nanowires and nanotubes is becoming very relevant and important. Indeed, the electronic property of nanowire and nanotube networks has been studied via percolation theory [17]. As for the thermal conductivity, it is found that even if the thermal conductivity of a single nanotube is very high, a system consisting of a three-dimensional random array of nanotubes shows an extremely low value of thermal conductivity [18]. However, compared with the electric properties, much less is known for heat conduction in complex networks.

In this work, we will study heat conduction in complex networks. In particular, we will focus on how the degree of a complex network, i.e., the number of links, affects the heat conduction behavior. In our model, the links between nodes are 1D chains of atoms represented by the FPU chain. This is very different from a previous model where the connection between two nodes is just a spring [19]. With this model, we show that the network structure can significantly influence the heat flux and temperature distribution. Theoretical analysis will be presented to understand the numerical results.

The remainder of the paper is organized as follows. In Sec. II we construct the network model to represent the nanotube and nanowire networks, with nodes forming a random network and links being 1D chains of atoms. In Sec. III we present the results of the numerical simulations of our quantities of interest such as the heat flux, the temperature distribution, and the thermal rectification. Theoretical analysis is provided to explain the

*zhliu@phy.ecnu.edu.cn

†baowen.li@colorado.edu

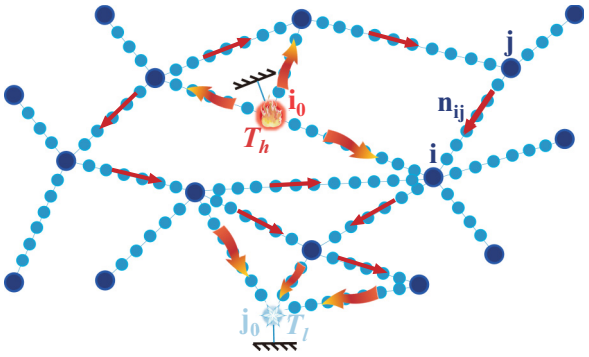

FIG. 1. Schematic picture of a complex network model, where the dark blue solid circles represent the nodes, the blue solid circles denote the atoms on links, i_0 and j_0 represent the two heat source nodes contacting two thermostats with high temperature T_h and low temperature T_l, respectively, and n_{ij} represents the number of atoms between the two connected nodes i and j.

numerical results. We finally summarize our main results in Sec. IV and conclude with a discussion.

II. THE NETWORK MODEL

The network model is constructed to represent the nanotube and nanowire networks, with nodes forming a random network and links being 1D chains of atoms. The random network is obtained by the approach in Ref. [20], with size N (number of nodes) and average degree $\langle k\rangle$(average degree of nodes). Figure 1 shows a schematic picture where the dark blue solid circles represent the nodes, the blue solid circles denote the atoms on the links, the fire and snow represent the two source nodes i_0 and j_0 contacting the Langevin heat baths with high temperature T_h and low temperature T_l, respectively, and n_{ij} denotes the number of atoms on a link $i \leftrightarrow j$. It is clear that each atom on a link is connected only to its two nearest neighbors, while the atom at node i is connected to its k_i nearest neighbors.

For simplicity, we let the atoms at both the nodes and links be the same one with the Hamiltonian

$$H = \sum_i \left[\frac{1}{2}p_i^2 + V_i(x_i)\right] \tag{1}$$

and the potential

$$V_i(x_i) = \frac{1}{2}\sum_{l=1}^{k_i}\left[\frac{1}{2}(x_i - x_l)^2 + \frac{\beta}{4}(x_i - x_l)^4\right], \tag{2}$$

where i runs through all the atoms on the network, x_i represents the displacement from the equilibrium position of the ith atom, k_i is the number of links connecting the ith atom, and β is the normalized nonlinear constant, which is 1 in this paper; that is, each link is considered as a 1D FPU-β chain [1].

We should mention that the 1D FPU model (or any other nonlinear lattice models of a 1D chain of atoms) is very different from realistic nanowire and/or nanotubes, not only in atomic structures but also in vibration modes. For example, for a 1D lattice model only vibration in longitudinal direction is considered; the transverse vibrations are usually neglected. Moreover, in the 1D lattice model, the atom has only two nearest neighbor atoms, whereas in the real nanowire or nanotube, there are more than two nearest neighbor atoms. These are the detailed structure differences.

However, we should point out one important fact: that the heat conduction behavior of a 1D nonlinear atomic chain is quite similar to that of a nanowire and nanotube. For example, generally in a 1D momentum-conserved system, such as the FPU model, the thermal conductivity κ diverges with the length of the system as $\kappa \sim L^{\xi}$, where ξ is a positive value that varies from model to model, but it is between 0.3 and 0.5 [1,2]. A numerical simulation for a single-wall nanotube and nanowire also shows similar behavior, in both the nanowire and nanotube; the thermal conductivity also diverges with nanotube or nanowire length as $\kappa \sim L^{\xi}$, ξ varies also from system to system. For details, refer to Ref. [7] for nanowire, Ref. [5] for nanotubes (numerical simulation), and Ref. [6] (experiment). More about heat conduction properties for 1D models and quasi-1D materials behavior can be found in the review [8].

In our simulations, fixed boundary conditions for two nodes i_0 and j_0 that attached to the two heat baths are used (see Fig. 1). The heat bath is modeled by a stochastic Langevin heat bath. The coupling strength is determined by the friction coefficient γ in Langevin dynamics; $\gamma = 4$ in this paper. This value is within the range of $\gamma \in (1, 100)$ recommended by Chen *et al.* [21] so that a meaningful physics can be obtained.

The equation of motions of the other nodes follow the canonical equations

$$\frac{dp_i}{dt} = -\frac{\partial H}{\partial x_i}. \tag{3}$$

Let the Langevin heat baths act on the i_0 and j_0 nodes, keeping them at temperatures T_h and T_l, respectively. Therefore, they satisfy

$$\frac{dp_h}{dt} = -\frac{\partial H}{\partial x_h} + \Gamma_h - \gamma p_h, \tag{4}$$

$$\frac{dp_l}{dt} = -\frac{\partial H}{\partial x_l} + \Gamma_l - \gamma p_l, \tag{5}$$

where $\Gamma_{h,l}$ are the Gaussian white noises with

$$\begin{aligned}\langle\Gamma_{h,l}(t)\rangle &= 0,\\ \langle\Gamma_h(t)\Gamma_h(0)\rangle &= 2\gamma k_B T_h\delta(t),\\ \langle\Gamma_l(t)\Gamma_l(0)\rangle &= 2\gamma k_B T_l\delta(t),\end{aligned} \tag{6}$$

where k_B is the Boltzmann constant, and we adopt the dimensionless unit by setting $k_B = 1$.

After an integration of 10^6 dimensionless time units with a time step of 0.01, the network will reach a stationary state. The local temperature at each atom can be defined as $T(i) = \langle p_i^2\rangle$, and the heat flux along the chain is $J_i = \langle \dot{x}_i \partial V/\partial x_{i+1}\rangle$ [13].

III. THE RESULTS

In our numerical simulations, we let $N = 50$, $T_h = 1.0$, $T_l = 0.1$, and $n_{ij} = 5$ for all the links in this work unless otherwise stated. We randomly choose two nodes as the source nodes that are attached to the high- and low-temperature thermal baths, respectively. The stationary heat flux J of a network is the sum on all the paths from node i_0 to its neighbors or the sum on all the paths to node j_0. It is found that the flux J depends sensitively on the degree of the two

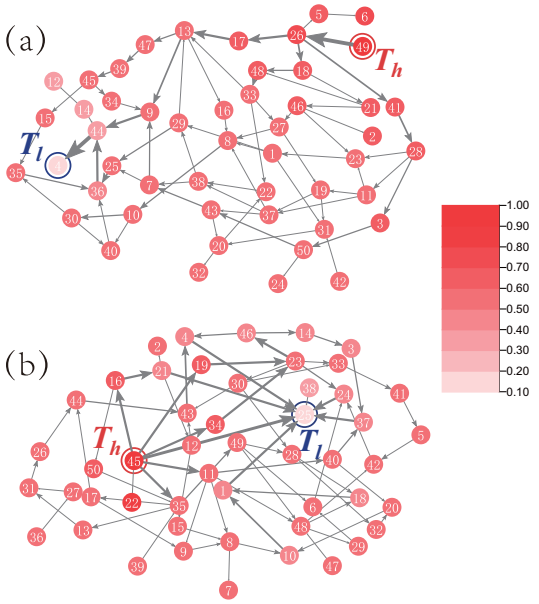

FIG. 2. Heat fluxes in a random network with average degree $\langle k\rangle = 3$. The length between two nodes is fixed at $n_{ij} = 5$. (a) Source nodes 4 and 49 with only one link, i.e., $k_0 = 1$, are chosen as the high- and low-temperature node, respectively. (b) Source nodes 25 and 45 with seven links, i.e., $k_0 = 7$, are chosen as the high- and low-temperature heat source node, respectively. The thickness of the arrow indicates the magnitude of the heat flux. The arrows indicate the heat flux direction.

source nodes i_0 and j_0, k_{i_0} and k_{j_0}, respectively. Figures 2(a) and 2(b) show qualitatively the heat flux and the distribution of temperatures at nodes on links for two sets of heat source nodes, respectively, where the atoms on links are not shown for clarity and the arrows represent the directions of heat fluxes on links. Figures 2(a) and 2(b) schematically illustrate the significant difference of heat flux and temperature distribution when the degrees of the heat source nodes are different.

It is found that when the source nodes have an optimal degree, heat flux through the complex network is largest. To get a clearer picture, we systematically investigated how the degrees of the source nodes affect the heat flux. To make life easier, we let the two source nodes have the same degree: $k_{i_0} = k_{j_0} = k_0$. Figure 3(a) shows the dependence of $\langle J\rangle$ on k_0 where squares, circles, triangles, and antitriangles denote the cases of $\langle k\rangle = 3, 4, 5$, and 6, respectively, and $\langle J\rangle$ is an average over 20 realizations of network structures. It is easy to see that there is a maximum of the $\langle J\rangle$ at an optimal value of k_0, indicating that the source nodes with optimal degree k_0 favor the heat conduction, while the source nodes with smaller or larger degree k_0 do not favor the heat conduction.

This finding, at first glance, is somehow counterintuitive as we generally believed that heat flow will always increase with the increase of paths attached to the source nodes. However, it is understandable in terms of interfacial thermal resistance. Larger degree k_0 means more interfaces, thus larger interfacial thermal resistance. On the other hand, Fig. 3(b) shows the dependence of $\langle J\rangle$ on $\langle k\rangle$ where squares, circles, and triangles denote the cases of $k_0 = 1, 3$, and 5, respectively, and $\langle J\rangle$ is also an average on 20 realizations of network structures.

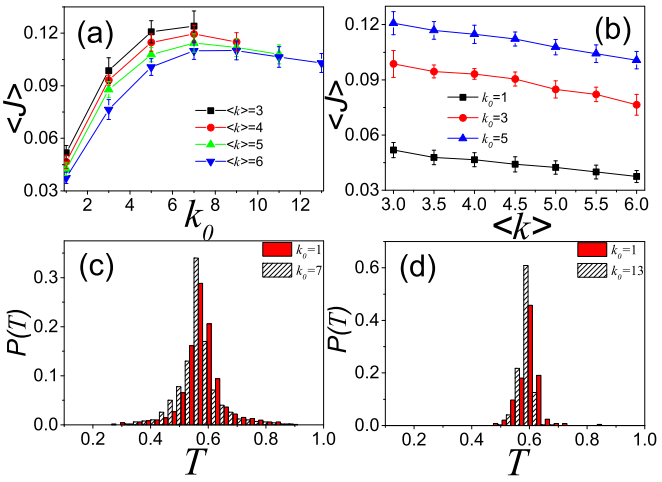

FIG. 3. Influence of the degree of two source nodes on heat conduction for averaging over 20 realizations. The length between two nodes is fixed at $n_{ij} = 5$. (a) $\langle J\rangle$ versus k_0 where squares, circles, triangles, and antitriangles denote the cases of $\langle k\rangle = 3, 4, 5$, and 6, respectively; (b) $\langle J\rangle$ versus $\langle k\rangle$ where squares, circles, and triangles denote the cases of $k_0 = 1, 3$, and 5, respectively; (c) and (d) $P(T)$ versus T for different values of k_0, where (c) is for the case of $\langle k\rangle = 3$ and (d) for $\langle k\rangle = 6$.

We can see that for the same degree k_0, the $\langle J\rangle$ decreases monotonically with the increase of $\langle k\rangle$, i.e., $\langle J\rangle$ in the sparse network of Fig. 3(b) with smaller $\langle k\rangle$ is larger than that in the dense network with larger $\langle k\rangle$, indicating that the sparse network with smaller $\langle k\rangle$ is more favorable to heat flux. While the $\langle k\rangle$ is fixed, the $\langle J\rangle$ increases as the k_0 increases, further confirming the effect that smaller k_0 is not favorable for heat conduction.

To gain a further understanding, we show the distribution $P(T)$ of nodes' temperatures for different k_0 in Figs. 3(c) and 3(d) with $\langle k\rangle = 3$ and 6, respectively. We see that the $P(T)$ will become narrower when $\langle k\rangle$ increases, indicating that the larger the degrees, the more interfaces we find, and thus the more difficult for heat flow. This may be because as more nanotubes or nanowires are interconnected in one node, more phonons will be backscattered [22,23]. Furthermore, the similar results for $n_{ij} = 5$ can also occur if we assume n_{ij} to be a random number from a uniform distribution and satisfies $1 \le n_{ij} \le 9$ (see Fig. 8 in the Appendix).

To understand the heat conduction mechanism in Fig. 3, we turn to a simplified theory. The simplified theoretical analysis reflects only the influence of network topology but neglects other aspects such as the atoms on links and the interface resistance. We let the coupling strength between the nodes i and j be c_{ij}, thus the adjacency matrix will be $C = (c_{ij})$ with $c_{ij} = 1$ if i and j are connected and 0 otherwise. Let $c_{ii} = 0$ for avoiding self-connection. Denote $\mathbf{F}$ as the temperature vector of N components. For convenience, we reorganize the network and let the source with T_h be node 1 and the sink with T_l be node 2. Then the temperature vector $\mathbf{F}$ can be expressed as $\mathbf{F} = (T_h, T_l, T_3, \ldots, T_N)^T$ and can be divided into block 1 with $\mathbf{F}_1 = (T_h, T_l)^T$ and block 2 with $\mathbf{F}_2 = (T_3, \ldots, T_N)^T$:

$$F = \begin{pmatrix} F_1 \\ F_2 \end{pmatrix}. \tag{7}$$

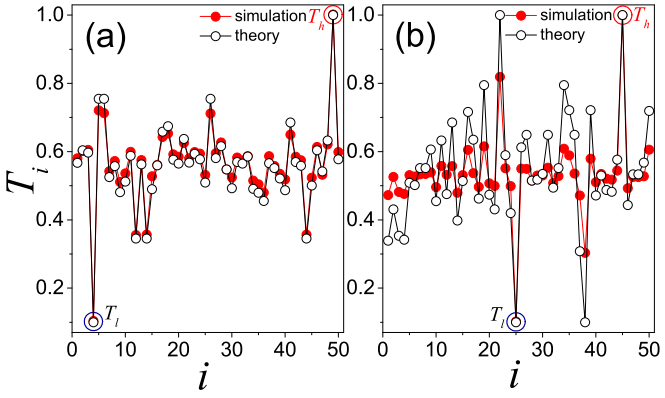

FIG. 4. Comparison between the numerical simulations (solid circles) of Fig. 2 and theoretical analysis (open circles) of Eq. (9) with average degree $\langle k\rangle = 3$. (a) Source nodes 4 and 49 with only one link, i.e., $k_0 = 1$, are chosen as the high- and low-temperature node, respectively. (b) Source nodes 25 and 45 with seven links, i.e., $k_0 = 7$, are chosen as the high- and low-temperature heat source node, respectively.

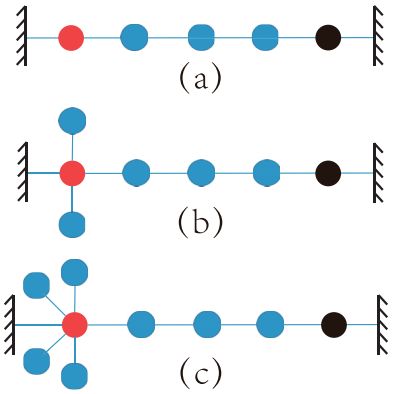

FIG. 5. Schematic picture of a simple network structure, where the red (left) and black (right) solid circles represent the two heat source nodes. (a) 2 and 2 degrees of the heat source nodes; (b) 4 and 2 degrees of the heat source nodes; and (c) 6 and 2 degrees of the heat source nodes.

The discrete Laplace operator on the network, an analog of ∇^2 is $L = I - P$ with $I = (\delta_{ij}k_i)$ and $P = D^{-1}C$, where D is the diagonal degree matrix. Correspondingly, the matrix L can be divided into four submatrices L_{11}, L_{12}, L_{21}, and L_{22}. In the steady state, we have

$$L\,\mathbf{F} = \mathbf{J}, \tag{8}$$

where $\mathbf{J}$ is the external flux vector. Note that this is the discrete analog of $-\kappa\nabla^2\mathbf{T}(\mathbf{r}) = \nabla\cdot\mathbf{j}(\mathbf{r})$ with $\mathbf{F}$ playing the role of $\kappa\mathbf{T}(\mathbf{r})$ and $\mathbf{J}$ playing the the role of $-\nabla\cdot\mathbf{j}(\mathbf{r})$, where $\mathbf{j}(\mathbf{r})$ is the flux vector field. Except for the source and sink nodes, the equilibrium condition demands that no net heat flux should occur, namely, $\mathbf{J} = 0$ for the nodes $i = 3, \ldots, N$. Hence we have

$$\begin{pmatrix} L_{11} & L_{12} \\ L_{21} & L_{22} \end{pmatrix}\begin{pmatrix} F_1 \\ F_2 \end{pmatrix} = \begin{pmatrix} J \\ 0 \end{pmatrix}. \tag{9}$$

From Eq. (9) we can get the temperature distribution $\mathbf{F}_2$. In this way, the open circles in Figs. 4(a) and 4(b) show the results for $\langle k\rangle = 3$. For comparison, we also put there the numerical results of the corresponding Figs. 2(a) and 2(b) (solid circles). It is easy to see that the theoretical and numerical results have the same variation tendency, indicating that the simple theory do explain the influence of network topology. The shift between the numerical and theoretical results will enlarge with the increasing of k_0; this may be because theoretical analysis neglects the interfacial thermal resistance.

The above results are obtained for the case of constant n_{ij} at all the links. In the nanotube and nanowire networks, n_{ij} will be quite different from link to link, but its heat conduction can be still investigated by this physical network model. This model can be also extended to the case with multiple high-temperature source nodes or multiple low-temperature source nodes.

Thermal rectification is one important physical phenomenon discovered in past decades [24]. This nonreciprocal transport phenomenon due to asymmetric interfacial thermal resistance [25] has been confirmed in many nanostructure systems [3,13]. Here we illustrate that the asymmetric degree connection with the heat sources can also induce thermal rectification in simple networks. This provides one additional dimension for thermal management. Figures 5(a)–5(c) show the schematic pictures of the simple network structures, where the red and black solid circles represent the two heat source nodes contacting the Langevin heat baths. Here the asymmetric structure is generated by adding nodes to the left red source node, but the structure of the right black source node is unchanged, i.e., 2/2 (representing the degree of left and right heat source nodes, respectively) for the left and right heat source nodes in Fig. 5(a), 4/2 in Fig. 5(b), and 6/2 of the heat source nodes in Fig. 5(c).

To make it clearer, we let the smaller and larger degrees of the two source nodes be k_s and k_l, respectively. Without loss of generality, we let $k_s = 2$ and only change $k_l (\geq k_s)$. Then we let J_+ (J_-) represent the network flux when k_s (k_l) and k_l (k_s) are chosen as the two source nodes with higher temperature T_h and lower temperature T_l, respectively. Figure 6(a) shows the dependences of J_+ versus k_l (solid circles) and J_- versus k_l (open circles). It is easy to see that J_+ and J_- decrease, and behave quite differently, and their difference increases

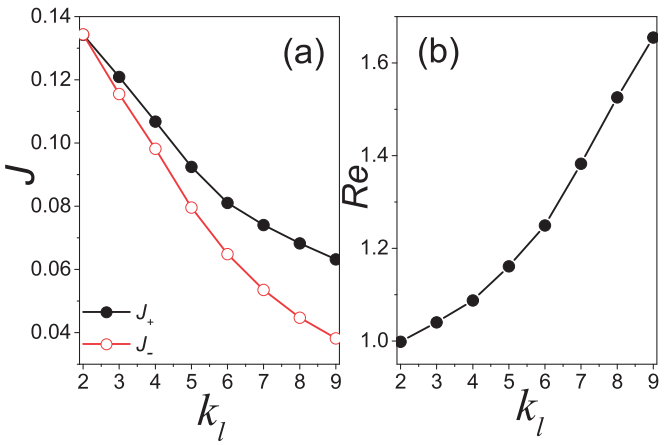

FIG. 6. Effect of rectification for $k_s = 2.0$. (a) J_+ versus k_l (solid circles), and J_- versus k_l (open circles); (b) R_e versus k_l.

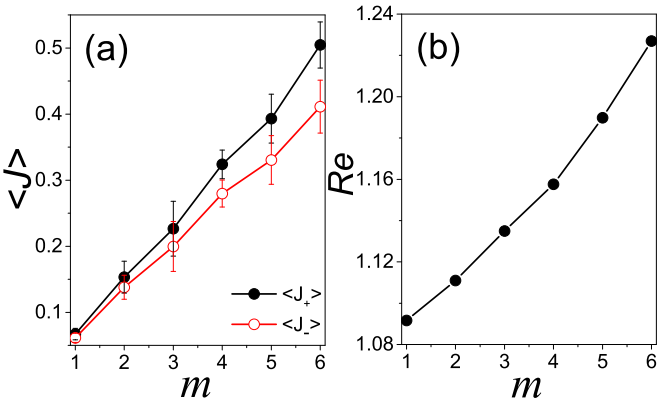

FIG. 7. Effect of rectification for $\langle k\rangle = 2$ and averaging on 20 realizations. (a) $\langle J_+\rangle$ versus m (solid circles) and $\langle J_-\rangle$ versus m (open circles); (b) R_e versus m.

monotonically with k_l, indicating that there exists an effect of rectification. We define the rectification coefficient as

$$R_e = \frac{J_+}{J_-}. \tag{10}$$

Figure 6(b) shows the dependence of R_e on k_l. We see that the R_e increases as the k_l increases, indicating that the larger k_l is favorite the thermal rectification. In the carbon nanotube network, a measurable quantity is the network density, defined as the number of nanotubes per unit area [26]. Therefore, Fig. 6(b) represents the cases of different simple network structures, and their confirmation can be expected in experiments.

We can obtain the range of frequency $f_i = \omega_i/2\pi$ as

$$0 < f_i < \frac{1}{\pi}\sqrt{\frac{k_i}{2}}. \tag{11}$$

Thus, we have $0 < f_i < 0.32$ for $k_i = 2$, which is consistent with the result in a 1D lattice [24]. The detailed discussion of f_i is presented in the Appendix. To confirm the phonon band in Eq. (11), we make power spectra from source nodes' time series in Fig. 5. The theoretical results are $f_{k_i=2} = 0.32$ for $k_i = 2$, $f_{k_i=4} = 0.45$ for $k_i = 4$ and $f_{k_i=6} = 0.55$ for $k_i = 6$, which is consistent with the power spectra (see Fig. 10 in the Appendix).

We now use Eq. (11) to explain the rectification. For the J_+ from k_s to k_l, its phonon diffusion is from narrow frequency to wide frequency. As the narrow phonon band is within the wide phonon band, it is easy for the heat flux to be sent from T_h to T_l. While for the J_- from k_l to k_s, its phonon diffusion is from wide frequency to narrow frequency. In this case, only part of the wide phonon band overlaps with the narrow phonon band, and thus only part of the heat flux from the source node with high temperature T_h can be sent to the source node with low temperature T_l, which results in $J_+ > J_-$ and thus the rectification effect.

Finally, we extend the above simple cases with two source nodes to some complicated cases with more than two source node, where $2m$ source nodes with the largest and smallest degrees contact T_h and T_l, respectively. Figures 7(a) and 7(b) show the dependences of $\langle J_\pm\rangle$ and R_e on m for the sparse network ($\langle k\rangle = 2$), respectively. It is seen that $\langle J_+\rangle$ and $\langle J_-\rangle$ increase and behave quite differently, and their difference increases monotonically with m, indicating that the larger m favors the thermal rectification. But for the dense network (i.e., larger $\langle k\rangle$), it should be pointed out that the thermal rectification disappears (figure not shown here). This may be the case that larger $\langle k\rangle$ will weaken the asymmetry of the network structure and thus results in the disappearance of thermal rectification. In addition, the similar results for $n_{ij} = 5$ can also occur if we assume n_{ij} to be a random number from a uniform distribution and satisfies $1 \le n_{ij} \le 9$ (see Fig. 9 in the Appendix).

IV. CONCLUSION AND DISCUSSION

In summary, we have presented a network model to study heat conduction in nanotube and nanowire networks. With this model we find that heat flux is seriously influenced by the chosen source nodes. The larger degree of source nodes does not prefer heat conduction, instead it reduces the heat flux. A dense network can reduce heat flux more than the sparse network. On the other hand, thermal rectification has been found when the degrees of the two source nodes are different. The rectification will be significant when the degree difference between the two source nodes becomes large or the network model has more heat source nodes. A simplified theory is provided to explain the numerical results.

ACKNOWLEDGMENTS

This work was partially supported by the NNSF of China under Grant Nos. 11675056 and 11375066, the Candidate Talents Training Fund of Yunnan Province (Project No. 2015HB025 and 11665014), and the Natural Science Foundation of Yunnan Province (under Project No. 2017FB003).

C.Z. and K.X. contributed equally to this work.

APPENDIX

Differently from the case of $n_{ij} = 5$, here we assume n_{ij} to be a random number from a uniform distribution and satisfies $1 \le n_{ij} \le 9$, which is shown in Figs. 8 and 9.

Figure 8(a) shows the dependence of $\langle J\rangle$ on k_0 where squares, circles, triangles, and antitriangles denote the cases of $\langle k\rangle = 3$, 4, 5, and 6, respectively, and $\langle J\rangle$ is an average over 20 realizations of network structures. It is easy to see that there is a maximum of $\langle J\rangle$ at an optimal value of k_0, indicating that the source nodes with optimal degree k_0 favor the heat conduction, while the source nodes with smaller or larger degree k_0 do not favor the heat conduction. Figure 8(b) shows the dependences of $\langle J\rangle$ on $\langle k\rangle$ where squares, circles, and triangles denote the cases of $k_0 = 1$, 3, and 5, respectively, and $\langle J\rangle$ is an average over 20 realizations of network structures. We can see that for the same degree k_0, $\langle J\rangle$ decreases monotonically with the increase of $\langle k\rangle$, i.e., $\langle J\rangle$ in the sparse network of Fig. 8(b) with smaller $\langle k\rangle$ is larger than that in the dense network with larger $\langle k\rangle$, further confirming the effect that larger k_0 does not favor heat conduction. To gain a further understanding, we show the distribution $P(T)$ of nodes' temperatures for different k_0 in Figs. 8(c) and 8(d) with $\langle k\rangle = 3$ and 6, respectively. We see that the $P(T)$ will become narrower when k_0 or $\langle k\rangle$ increases, indicating that the larger the degrees, the more the interfaces, thus the more difficult for heat flow. Comparing with Fig. 3, we

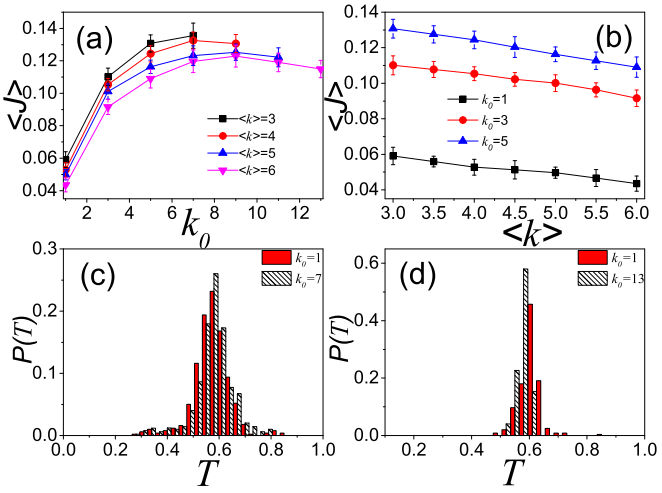

FIG. 8. Influence of the degree of two source nodes on heat conduction for averaging over 20 realizations. Differently from Fig. 3, here n_{ij} is (uniform) randomly distributed in $1 \leq n_{ij} \leq 9$. (a) $\langle J \rangle$ versus k_0 where squares, circles, triangles, and antitriangles denote the cases of $\langle k \rangle = 3$, 4, 5, and 6, respectively; (b) $\langle J \rangle$ versus $\langle k \rangle$ where squares, circles, and triangles denote the cases of $k_0 = 1$, 3, and 5, respectively; (c, d) $P(T)$ versus T for different values of k_0, where (c) is for the case of $\langle k \rangle = 3$ and (d) for $\langle k \rangle = 6$.

see that the results of the Fig. 8 for $1 \leq n_{ij} \leq 9$ is consistent with the results of Fig. 3 for $n_{ij} = 5$.

Figures 9(a) and 9(b) show the dependences of $\langle J_{\pm} \rangle$ and R_e on m for the sparse network ($\langle k \rangle = 2$), respectively. It is easy to see that $\langle J_+ \rangle$ and $\langle J_- \rangle$ increase and behave quite differently, and their difference increases monotonically with m, indicating that the larger m favors the thermal rectification. But for the dense network (larger $\langle k \rangle$), it should be pointed out that the thermal rectification disappears (figure not shown here). Comparing with Fig. 7, we see that the results of Fig. 9 for $1 \leq n_{ij} \leq 9$ is consistent with the results of Fig. 7 for $n_{ij} = 5$.

To understand the underlying mechanism of rectification, we make a brief theoretical analysis. We have equations of

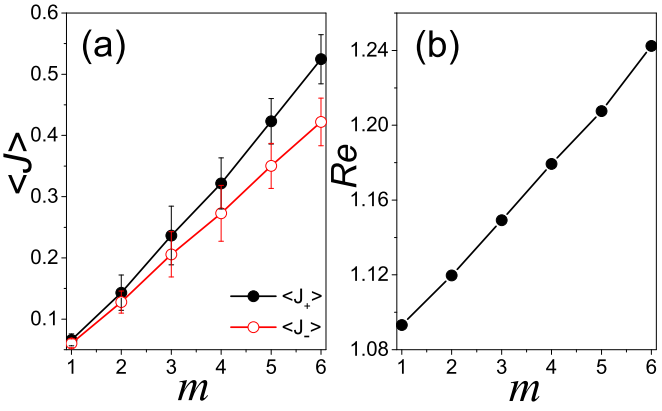

FIG. 9. Effect of rectification for $\langle k \rangle = 2$ and averaging over 20 realizations. Differently from Fig. 7, here n_{ij} is (uniform) randomly distributed in $1 \leq n_{ij} \leq 9$. (a) $\langle J_+ \rangle$ versus m (solid circles), and $\langle J_- \rangle$ versus m (open circles); (b) R_e versus m.

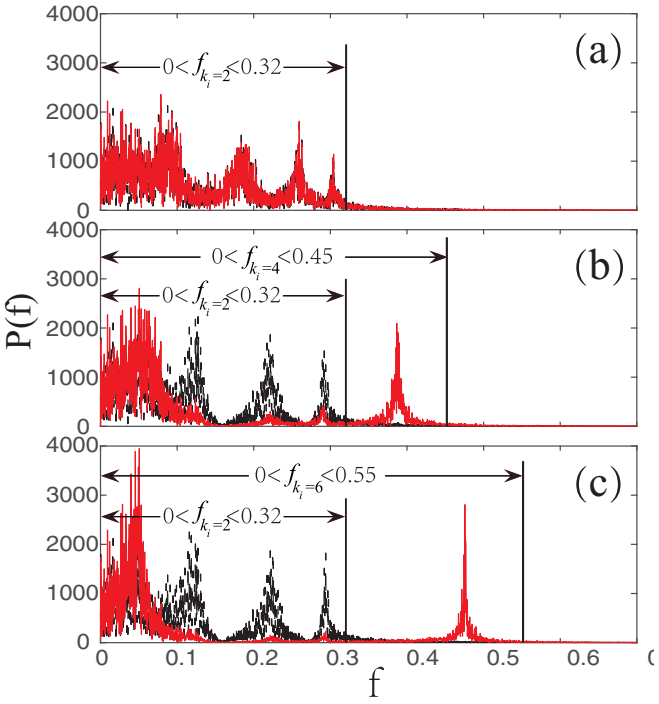

FIG. 10. Power spectra of two heat source nodes of the corresponding Fig. 5. (a) 2 and 2 degrees of the heat source nodes, (b) 4 and 2 degrees of the heat source nodes, and (c) 6 and 2 degrees of the heat source nodes, respectively.

motion:

$$\ddot{x}_i = -\frac{\partial V_i(x_i)}{\partial x_i} - \sum_{j=1}^{k_i} \frac{\partial V_j(x_j)}{\partial x_i}, \tag{A1}$$

where the first and second terms on the right-hand side of Eq. (A1) come from the potentials of node i and its neighbors, respectively. Substituting Eq. (2) into Eq. (A1) we have

$$\ddot{x}_i = -\sum_{j=1}^{k_i} [(x_i - x_j) + \beta (x_i - x_j)^3]. \tag{A2}$$

When the amplitude of x_i is small, we may neglect the nonlinear term in Eq. (A2) and thus obtain

$$\ddot{x}_i = \sum_{j=1}^{k_i} (x_j - x_i). \tag{A3}$$

Equation (A3) has plane wave solutions $x_i = e^{I(q_i z_i - \omega_i t_i)}$ and $x_j = e^{I(q_j z_j - \omega_j t_j)}$, where I represents the imaginary unit. Substituting them back to Eq. (A3), we obtain the relationship between the frequency ω_i and degree k_i as

$$\omega_i = \sqrt{\sum_{j=1}^{k_i} [1 - \cos(q_j z_j - q_i z_i + \phi)]}, \tag{A4}$$

in which $\phi = \omega_i t_i - \omega_j t_j$ is a constant.

Therefore, we can obtain the range of frequency $f_i = \omega_i / 2\pi$ as

$$0 < f_i < \frac{1}{\pi} \sqrt{\frac{k_i}{2}}. \tag{A5}$$

Figure 10 shows the power spectra from source nodes' time series of the corresponding Fig. 5, i.e., 2 and 2 degrees of the heat source nodes in Fig. 10(a), 4 and 2 degrees of the heat source nodes in Fig. 10(b), and 6 and 2 degrees of the heat source nodes in Fig. 10(c). The theoretical results are $f_{k_i=2} = 0.32$ for $k_i = 2$, $f_{k_i=4} = 0.45$ for $k_i = 4$ and $f_{k_i=6} = 0.55$ for $k_i = 6$, which is consistent with the power spectra in Fig. 10.

[1] S. Lepri, R. Livi, and A. Politi, Phys. Rep. **377**, 1 (2003).
[2] A. Dhar, Adv. Phys. **57**, 457 (2008).
[3] N. Yang, X. Xu, G. Zhang, and B. Li, AIP Adv. **2**, 041410 (2012).
[4] D. G. Cahill, P. V. Braun, and G. Chen *et al.*, J. Appl. Phys. Rev. **1**, 011305 (2014).
[5] S. Maruyama, Physica B **323**, 193 (2002).
[6] C. W. Chang, D. Okawa, H. Garcia, A. Majumdar, and A. Zettl, Phys. Rev. Lett. **101**, 075903 (2008).
[7] N. Yang, G. Zhang, and B. Li, Nano Today **5**, 85 (2010).
[8] S. Liu, X.-F. Xu, R.-G. Xie, G. Zhang, and B. Li, Eur. Phys. J. B **85**, 337 (2012).
[9] D. S. Sato, Phys. Rev. E **94**, 012115 (2016).
[10] L. Wang, B. Hu, and B. Li, Phys. Rev. E **86**, 040101 (2012).
[11] G. Fugallo, A. Cepellotti, and L. Paulatto *et al.*, Nano. Lett. **14**, 6109 (2014).
[12] X. Xu, L. F. C. Pereira, and Y. Wang *et al.*, Nat. Commun. **5**, 3689 (2014).
[13] N. Li, J. Ren, L. Wang, G. Zhang, P. Hanggi, and B. Li, Rev. Mod. Phys. **84**, 1045 (2012).
[14] B. Y. Lee, M. G. Sung, and H. Lee *et al.*, NPG Asia Mat. **2**, 103 (2010).
[15] Q. Cao and J. A. Rogers, Adv. Mater. **21**, 29 (2009).
[16] D. R. Kauffman and A. Star, Angew. Chem. **47**, 6550 (2008).
[17] S. Kumar, J. Y. Murthy, and M. A. Alam, Phys. Rev. Lett. **95**, 066802 (2005).
[18] R.S. Prasher, X.J. Hu, Y. Chalopin, N. Mingo, K. Lofgreen, S. Volz, F. Cleri, and P. Keblinski, Phys. Rev. Lett. **102**, 105901 (2009).
[19] Z. Liu, X. Wu, H. Yang, N. Gupte, and B. Li, New J. Phys. **12**, 023016 (2010).
[20] R. Albert and A. Barabasi, Rev. Mod. Phys. **74**, 47 (2002).
[21] J. Chen, G. Zhang, and B. Li, J. Phys. Soc. Jpn. **79**, 074604 (2010).
[22] J. K. Yu, S. Mitrovic, and D. Tham *et al.*, Nat. Nanotechnol. **5**, 718 (2010).
[23] M. Verdier, D. Lacroix, and K. Termentzidis, arXiv:1802.05654.
[24] B. Li, L. Wang, and G. Casati, Phys. Rev. Lett. **93**, 184301 (2004).
[25] B. Li, J.-H. Lan, and L. Wang, Phys. Rev. Lett. **95**, 104302 (2005).
[26] H. Xu, S. Zhang, S.M. Anlage, L. Hu, and G. Grüner, Phys. Rev. B **77**, 075418 (2008).